Mechanics and Mechanical Engineering
Vol. 22, No. 2 (2018) 619–635

https://doi.org/10.2478/mme-2018-0049

Numerical Analysis of the VAD Outflow Cannula Positioning on the Blood Flow in the Patient–Specific Brain Supplying Arteries

Zbigniew Tyfa
Damian Obidowski
Krzysztof Jóźwik

Institute of Turbomachinery
Lodz University of Technology
Lodz, Poland
zbigniew.tyfa@p.lodz.pl

Received (23 June 2018)
Revised (29 July 2018)
Accepted (26 September 2018)

The primary objective of this research can be divided into two separate aspects. The first one was to verify whether own software can be treated as a viable source of data for the Computer Aided Design (CAD) modelling and Computational Fluid Dynamics CFD analysis. The second aspect was to analyze the influence of the Ventricle Assist Device (VAD) outflow cannula positioning on the blood flow distribution in the brain-supplying arteries. Patient-specific model was reconstructed basing on the DICOM image sets obtained with the angiographic Computed Tomography. The reconstruction process was performed in the custom-created software, whereas the outflow cannulas were added in the SolidWorks software. Volumetric meshes were generated in the Ansys Mesher module. The transient boundary conditions enabled simulating several full cardiac cycles. Performed investigations focused mainly on volume flow rate, shear stress and velocity distribution. It was proven that custom-created software enhances the processes of the anatomical objects reconstruction. Developed geometrical files are compatible with CAD and CFD software – they can be easily manipulated and modified. Concerning the numerical simulations, several cases with varied positioning of the VAD outflow cannula were analyzed. Obtained results revealed that the location of the VAD outflow cannula has a slight impact on the blood flow distribution among the brain supplying arteries.

Keywords: VAD cannula, CFD, blood flow, patient-specific reconstruction.

1. Introduction

Currently, despite a rapid progress in the medical diagnostics and pharmacological fields, the number of people suffering from the vascular diseases, i.e. heart failure, is constantly increasing. Thus, the gap between the number of patients who require a heart transplantation and the number of possible heart donors is constantly expanding [1-3]. The only possible solution for some of the patients with the end-stage

heart failure is to undergo a surgical procedure, during which a left ventricular assist device (LVAD) is implanted. In general, the LVAD inflow cannula is located in the left ventricle, whereas the outflow cannula is anastomosed mainly to the ascending aorta - rarer locations comprise descending aorta or subclavian arteries [2, 4]. Such a device helps patients whose heart is working insufficiently (cannot pump the blood with the required cardiac output) by sustaining the continuous or pulsatile flow of the blood. The most optimal flow rate of majority of the continuous flow, LVADs available on the market which became more popular in adults treatment, ranges from 5 to 6 liters per minute [5], what provides almost the same output as the physiological cardiac output for the human organism at rest. Several publications devoted to the analysis of the LVAD on the blood flow assume slightly lower volume flow rate - approximately 4-5 liters per minute [4, 6, 7].

Despite the aforementioned paramount advantage of the LVADs, several negative phenomena might occur after the device implantation. Apart from the surgical complications or bleeding, the long-term usage of these devices might result with aortic valve insufficiency [8, 9], blood flow stagnation followed by clots formation or even higher rate of cerebrovascular adverse event rate [4, 10]. Therefore, numerous studies (either clinical, in-vitro or numerical) concerning the influence of the LVAD on the blood hemodynamics have been conducted. They were primarily focusing on the stagnation zones (blood clotting), turbulence investigations, thromboembolic events and wall shear stress distribution in the aortic arch [11-14]. Some of them were devoted to the comparable analysis of the wall shear stress and velocity changes or blood deficiency in the aortic arch due to different cannulas positioning [7, 15-18].

However, there is hardly any publication that outlines the impact of the LVAD cannula positioning on the blood distribution in the brain-supplying vessels, i.e. vertebral and carotid arteries. Specific anastomosis position and its angle might contribute to directing the main jet stream into one of the aortic branches (brachiocephalic trunk, left common carotid and left subclavian arteries) or to the descending aorta, leaving other arteries less supplied with the blood and more prone to the ischemic events. One publication found in literature presented the experimental results of the blood flow in the physical model, where in one of the brain-supplying arteries (right common carotid), the fluid had a negative direction. Instead of supplying the upper arteries and the brain, blood was sucked from those regions [4]. Presumably, this could lead to the negative flow in the cerebral circulation, resulting with the possible brain ischemia. The authors of this publication claim that such a phenomenon was related to the Venturi effect, assuming that the cannula was placed alongside the left subclavian artery [4].

Therefore, the main objective of the following research was to analyze the impact of the LVAD cannula anastomosis location on the blood distribution in the brain-supplying arteries with the use of numerical analyses (computational fluid dynamics, CFD).

2. Methodology

The investigated patient was recruited during the standard angiographic CT examination. He did not belong to the group of the patients suffering from the end-stage heart failure - he was examined since it was assumed that he had pathological

stenoses in the arterial system. Hence, the patient had a healthy heart that pumped the blood with the physiological frequency and cardiac output. Since the authors were in possession of the image dataset, it was decided to use those images to reconstruct the patient-specific geometry and assume that the patient's heart worked insufficiently. To follow the ethical standards, the patient provided written consent with the agreement of research and publication.

2.1. *Image processing and geometrical data extraction*

To investigate the influence of the LVAD outflow cannula positioning on the blood distribution among the brain supplying arteries, a specific 3D model had to be generated (starting from the aortic arch and ending at the basilar and internal carotid arteries). For that purpose, a custom-created, modified version of the MeMoS software, was used [19]. After importing a sequence of the DICOM images with the resolution equal to 0.488, 0.488 and 0.625 mm, the authors could start the image processing.

The general concept of the MeMoS software is to fill a binary spatial mask (of the same size as the loaded dataset) during semi-automatic or manual segmentation techniques. Afterwards, having the voxelated model (object made of cubes with the edge sizes equal to the image resolution), the software performs the marching cubes algorithm that extracts the surface of the given 3D mask. Additionally, the generated surface is smoothed in such a way that the overall topology is preserved, however, the surface is not any longer made of the cubes - it gets the higher smoothness. Simultaneously, the user can generate files comprising vessel centerline or its circumferential splines by selecting given points manually or with the use of active contour methods. Those data can be easily imported into any CAD software, for instance SolidWorks.

The first step of the proper image segmentation was to adjust the contrast and brightness of the images (*'windowing'* operation). Since MeMoS offers a vast amount of stored presets concerning the window level and window width, one could choose the angio-CT preset with the proper Hounsfield range.

The second step involved performing an automatic region growing algorithm. By sketching a line passing through the artery filled with the contrast agent, a Bresenham algorithm was triggered, assumed voxel-intensity range was calculated and the initial seed (starting point of the initial region) was estimated. As a result, the spatial mask was filled with the areas connected with the starting point whose intensity fell within the assumed intensity range. After the visual investigation of the created cross-sectional masks, it was decided to follow the region growing method by an active contour algorithm on the selected images (with the default parameters). As a result, the mask corresponded to the artery regions visible on the given image more precisely and more accurately. Nevertheless, the generated 3D mask required additional refinement and for that purpose, manual mask-filling algorithms were used, mainly lasso selector combined with the thresholding segmentation.

Simultaneously, numerous arrays representing the centerlines of the vessels were generated. After creating an empty array, the user was pinpointing the centroid of the vessel cross section and by clicking on that point, its coordinates were appended to the selected array. By repeating this procedure among dozens of images, a full

centerline of the given vessel was obtained. Having repeated the abovementioned procedure for each artery, centerlines of each branch of the investigated vessel tree network were generated.

2.2. *Model reconstruction and its refinement*

After the successful surface extraction and its initial smoothing, the authors had to prepare the model for the usage in the CFD software (Ansys CFX). Such a preparation required three main aspects. The first one was connected with the secondary smoothing, either with the default parameters or with the user-defined values. The second issue to be fulfilled was a removal of unnecessary branches and clipping of the areas near the outlets to obtain a boundary as perpendicular to the flow channel as possible. Otherwise, the volumetric mesh might be inappropriate, especially in the vicinity of the extremely narrow or high angles between adjacent faces (please see Figure 1). The last step involved the so-called 'capping' boundaries algorithm, during which the opened branch-ends were capped with the planar surfaces. They close the entire model, making a hollow object, and serve as the basis for the future boundary conditions assignments.

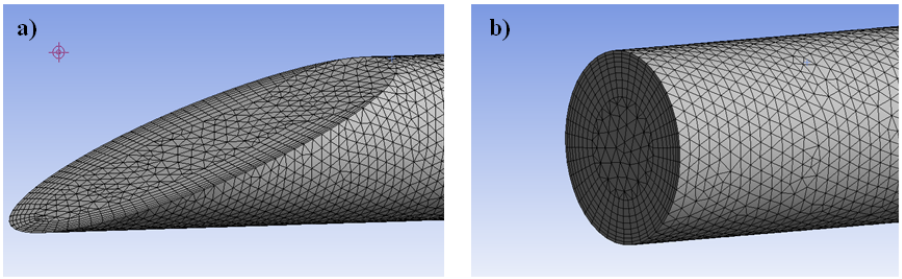

Figure 1 a) inappropriate mesh - improper angles between adjacent faces led to the break in the inflation layer continuity; b) appropriate mesh generated in the vicinity of the perpendicular outlet

At that point, the surface model was ready to be exported in the stereolitography format (STL) and meshed in the Ansys ICEM software. However, since the main objective of the following research was to analyze the impact of the LVAD outflow positioning on the blood distribution among brain-supplying arteries, it was decided not to use the STL files. Modifying the generated surface (making circular incision and protruding in-depth walls where the device should be implanted) and adding further geometrical objects to the STL file is extremely troublesome. Hence, the surface object was seed to the next module of the own software, MeMoS, where contour extraction takes place.

The general principle of contour extraction is to import the final surface object and all the required centerlines. By selecting a point on the vessel centerline, program automatically calculates a plane that is perpendicular to that spline. Simultaneously, a contour of the vessel wall is extracted – the generated plane intersects with the surface model and intersection points represent the artery contour. Such

a contour is stored as a separate array that can be exported in the format compatible with CAD software. After importing all the data (centerlines and artery contours) into SolidWorks software, an algorithm called 'profile-extrusion' was used to generate the volumetric object. Example figure depicting such a procedure is presented in Figure 2. By repeating this procedure for every artery, a complete 3D model was reconstructed.

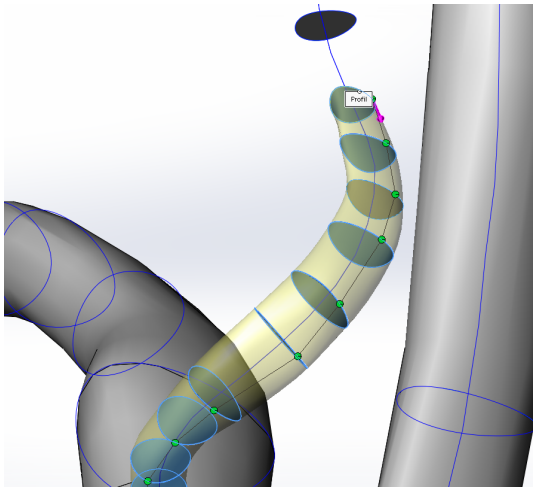

Figure 2 Procedure of generating the volumetric object in SolidWorks based on the data exported from the custom-created software (MeMoS)

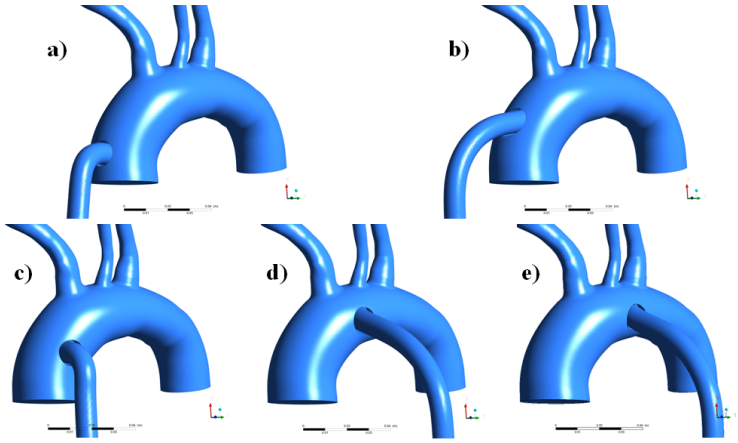

Figure 3 Investigated cases of different LVAD outflow cannula positioning investigated within this research

Considering the implantation of the LVAD outflow cannulas, artificial splines representing the pathway of this device were created. Five different cases were investigated (see Figure 3). In each analyzed case, the internal diameter of the cannula was assumed as 10.0 mm, whereas its wall thickness as 1.0 mm.

2.3. *Boundary conditions and blood model*

Blood is treated as a non-Newtonian fluid, so the strain dependent viscosity curve is non-linear. Since the blood viscosity can be influenced by numerous factors and it may vary among different populations (various geographical locations), several viscosity models can be found in the literature. During this research, a modified power law was used (governing equations listed below) [20-22]. The main advantage of this model is a fact that for higher shear strains it transforms into a Newtonian fluid. The density was assumed to be constant (equal to 1050 kg/m^3, which is a mean value of the range found in the literature [20, 21, 23, 24]) and since the temperature in the investigated arteries is constant, isothermal and adiabatic flow was assumed:

$$\begin{cases} \mu = 0.554712 & \text{for} \quad \left(2\frac{\partial U_i}{\partial x_j}S_{ij}\right)^{\frac{1}{2}} < 1e^{-9} \\ \mu = \mu_0\left(\left(2\frac{\partial U_i}{\partial x_j}S_{ij}\right)^{\frac{1}{2}}\right)^{n-1} & \text{for} \quad 1^{-9} \leq \left(2\frac{\partial U_i}{\partial x_j}S_{ij}\right)^{\frac{1}{2}} < 327 \\ \mu = 0.00345 & \text{for} \quad \left(2\frac{\partial U_i}{\partial x_j}S_{ij}\right)^{\frac{1}{2}} \geq 327 \end{cases} \tag{1}$$

where: μ – dynamic viscosity, μ_0 – reference viscosity (0.035 Pas) and $n = 0.6$ – constant.

The numerical simulations (Ansys CFX) were carried out as transient ones, where the boundary conditions vary in time. Considering the ratio between cardiac output to the aortic inflow for the patients with LVAD, it is claimed that only a small fraction of the blood volume is contributed by the heart, but the exact value is unknown and may vary among patients. It was assumed that the patient's heart operates significantly less sufficient but it generates weak pulses – the ascending aorta is supplied both through its anatomical inlet (around 10% of the total inflow, pulsating nature) and through the LVAD with uniform, constant volume flow rate equal to $7.5{\cdot}10^{-5}$ m^3/s (4.5 liter per minute). The transient boundary condition (at the inlet to the aorta), representing weakly operating heart, was based on the rescaled physiological values for the healthy patient to obtain the 10% of the overall inflow. Similar approach was used in the work of Karmonik et al. (2014), who assumed 5% of the total inflow through the aorta inlet. It is worth mentioning that the velocity profile distribution, known as Prandtl one-seventh power law, was assumed at the aorta inlet. Hence, the flow velocity is maximal at the vessel center and it continuously decreases while approaching the wall. Considering the boundary conditions for the outlets, they resemble the physiological values of the time-varying pressure. Such boundary conditions were taken from the literature and served as the basis for the other numerical analyses [21, 22]. Figure 4 outlines the time-dependent boundary conditions imposed on the specific regions in the domain. As far as a turbulence model is concerned, a Shear Stress Transport (SST) model was chosen.

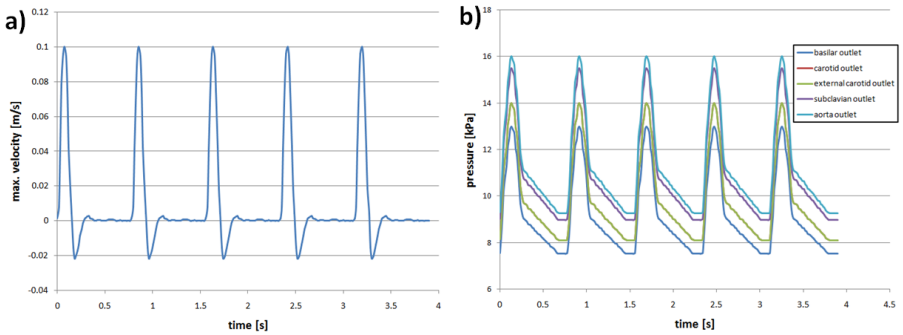

Figure 4 Transient boundary conditions: a) maximal velocity at the aorta inlet; b) pressure at specific arteries outlets [21, 22]

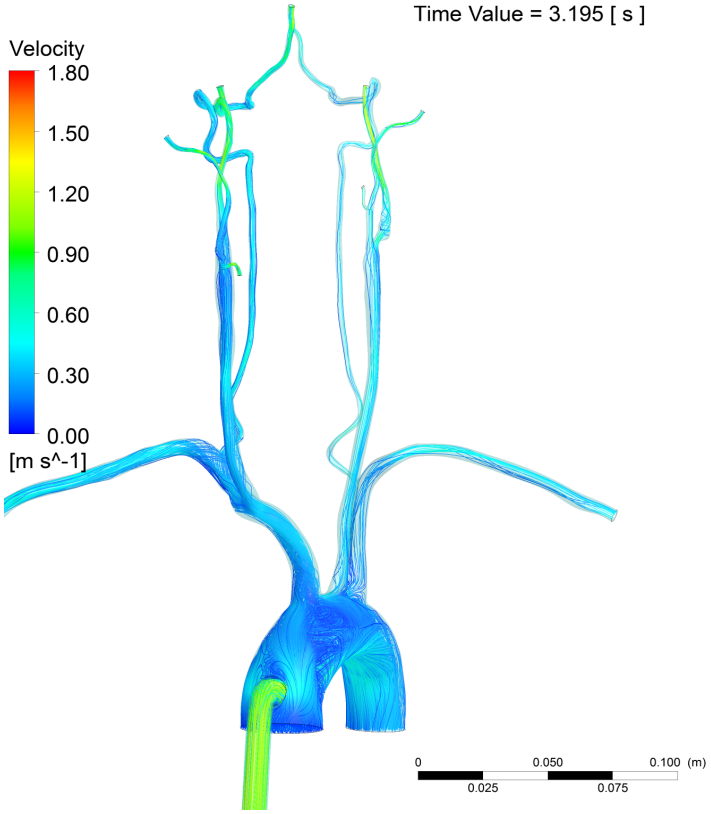

Figure 5 Velocity streamlines in the entire patient-specific model with the implanted LVAD outflow cannula; time step corresponds to the systole

Prior to performing the transient simulations, a parametric mesh independence test was conducted. Its purpose is to minimize the discretization error deriving from the mesh density. The maximal *GCI* parameter (describing the numerical uncertainty in the grid solution) for the finest and the middle meshes was equal to 3.91%. Hence, the middle-sized mesh, encompassing ca 7 million elements, was chosen for the further investigations. The minimal element size of such a mesh was equal to 0.05 mm, whereas the size of the maximal one could not exceed 1.5 mm. Table 1 outlines the parameters used and calculated during the mesh independence test.

Table 1 Discretization error of selected variables for three meshes of different densities

N_1 – 13 588 965 elements N_2 – 7 027 720 elements N_3 – 2 914 523 elements				r_{21} – 1.246 r_{32} – 1.341		
	ø - max. velocity in aorta [m/s]	ø - mass flow in aorta [kg/s]	ø - mass flow in left carotid artery [kg/s]	ø - mass flow in left external carotid artery [kg/s]	ø - average wall shear stress in the aortic arch [Pa]	ø - max. wall shear stress in the aortic arch [Pa]
$\emptyset_1$	0.39408	0.06220	0.00760	0.00147	1.409	10.586
$\emptyset_2$	0.38887	0.06152	0.00765	0.00149	1.457	10.239
$\emptyset_3$	0.39766	0.06004	0.00787	0.00154	1.611	9.099
p	1.969	1.876	4.526	2.410	3.350	3.439
$\emptyset_{ext}^{32}$	0.378	0.064	-0.008	-0.001	1.365	10.893
e_a^{32}	2.26%	2.40%	2.88%	3.36%	10.57%	11.13%
e_{ext}^{32}	2.98%	3.17%	1.05%	3.37%	6.75%	6.01%
$\emptyset_{ext}^{21}$	0.404	0.064	-0.008	-0.001	1.365	10.893
e_a^{21}	1.32%	1.09%	0.66%	1.36%	3.41%	3.28%
e_{ext}^{21}	2.38%	2.10%	0.39%	1.99%	3.23%	2.82%
GCI_{middle}^{32}	5.22%	5.89%	2.11%	6.01%	12.14%	12.32%
GCI_{fine}^{21}	3.05%	2.68%	0.48%	2.43%	3.91%	3.63%

3. Results

The patient-specific arterial model ranging from the aortic arch to the upper carotid arteries (both internal and external) and basilar artery were reconstructed. Reconstruction processes were performed in the custom-created program (modified version of MeMoS) and SolidWorks software. Afterwards, the LVAD outflow cannulas were added to the ascending aorta at 5 different positions. Due to the assumed pulsatile nature of the heart, all the analyses (further figures presented within this research) were taken for the systole, when the blood is ejected from the heart chamber and possesses the highest velocity. Figure 5 depicts a flow velocity distribution in the entire vessel tree network with the first alternation of the LVAD cannula (located at the bottom part of the ascending aorta).

As can be noticed, the global maximal velocity reaches the value of 1.8 m/s. However, such a fast blood flow is obtained only in the vicinity of the small arteries (short and narrow vessels) that are bifurcating from the proximal part of the internal carotid arteries. Thus, this slightly elevated velocity referred to physiological values, might result from the boundary condition imposed on the outlets of the aforementioned arteries and due to the negligence of some barely visible arteries in the images with limited spatial resolution. Nevertheless, the overall flow resembles the physiological hemodynamics of the blood. Moreover, as the blood flows through more distal arteries of the investigated system, its velocity is gradually increasing. This phenomenon is related to the constant reduction of the vessels diameters - when the channel gets narrower, there is a local increase in the velocity, what corresponds to the basic principle of the fluid mechanics (Bernouilli's principle).

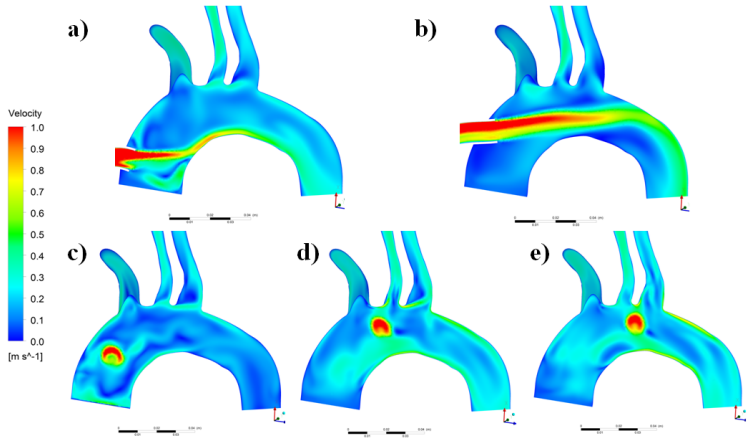

Figure 6 Velocity distribution in the aortic arch for each analyzed case of the LVAD cannula positioning at the systole (3.915 s)

Considering the influence of the LVAD cannula positioning on the blood flow in the aortic arch, significant changes can be observed, especially in the velocity (please see Figure 6). It can be noticed that the flow velocity as well as areas where the vortexes are present are different among all investigated cases. This phenomenon suggests that the blood might be distributed to the aortic branches in a varied manner. As a result, the brain-supplying arteries might deliver insufficient volume of the blood to the brain, what may result with the possible ischemia. Therefore, it was decided to carry out the analysis of the time-dependent volume flow rate at all the arteries that are supplying the brain. For that purpose, all the required data for the cross sections at the vertebral (left and right) and internal carotid (left and right) arteries were gathered. A graphical representation of the volume flow rate in the left internal carotid artery is depicted in the form of the plot (please see Figure 7). It was decided not to present plots for each analyzed artery due to similar characteristics in each case. However, a table comprising the integral of the volume

flow rate over the course of one full cardiac cycle for 5 different configurations of the cannula positioning is outlined in Table 2.

As stated before, basing on the images depicted in Figure 6, one can observe the velocity and vortex-areas changes between all of the investigated cases. Apart from the case 6b, where the cannula jet stream is directed towards the distal wall of the descending aorta, one can observe highly unordered and swirling flow in every analyzed case.

Table 2 Blood volume that flows at the different brain-supplying arteries over 1 full cardiac cycle

	Artery	VAD a	VAD b	VAD c	VAD d	VAD e
Area averaged volume flow rate [cm^3/s]	Right vertebral	1.27	1.26	1.28	1.27	1.27
	Left vertebral	1.87	1.80	1.89	1.88	1.88
	Right internal carotid	3.88	3.66	3.92	3.90	3.92
	Left internal carotid	3.70	3.53	3.72	3.71	3.71
Difference between obtained value and the average value	Right vertebral	0.26%	0.92%	1.04%	0.34%	0.21%
	Left vertebral	0.48%	3.48%	1.37%	0.84%	0.80%
	Right internal carotid	0.62%	5.08%	1.66%	1.19%	1.62%
	Left internal carotid	0.86%	4.01%	1.31%	0.93%	0.93%

As can be seen from the plot in Figure 7 and from the data presented in Table 2, blood volume discrepancies among all investigated cases are relatively small. Hence, despite modifying the position of the LVAD outflow cannula, the overall blood distribution among the brain-supplying arteries remains almost constant. The highest differences were mainly for VAD b (geometry where the cannula is implanted at the higher position in the ascending aorta) and exceeded the value of 5%, whereas the differences between other cases were ca 1%. Such small differences can be treated as negligible.

Figure 8 presents the wall shear stress (WSS) distribution at the aortic arch walls. It can be observed that elevated WSS values are present in the areas where the jet stream from the cannula hits the vessel wall. Thus, location of the areas subjected to high shear stresses depend on the cannula positioning. Since the physiological WSS for the aorta is claimed to be in the range 0.35-1.00 Pa [9, 25], the obtained values seem to be non-physiological and might contribute to severe problems with the patient's health, e.g. vessel remodeling, weakening of the vessel wall and possible formation of the aneurysm [9, 22, 26, 27].

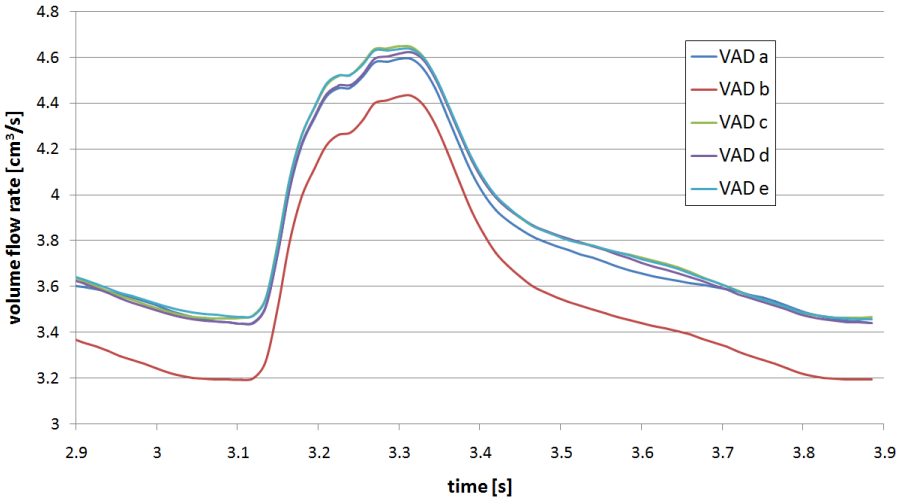

Figure 7 Area averaged volume flow rate in the left internal carotid artery - comparison between different cases of the LVAD cannula positioning

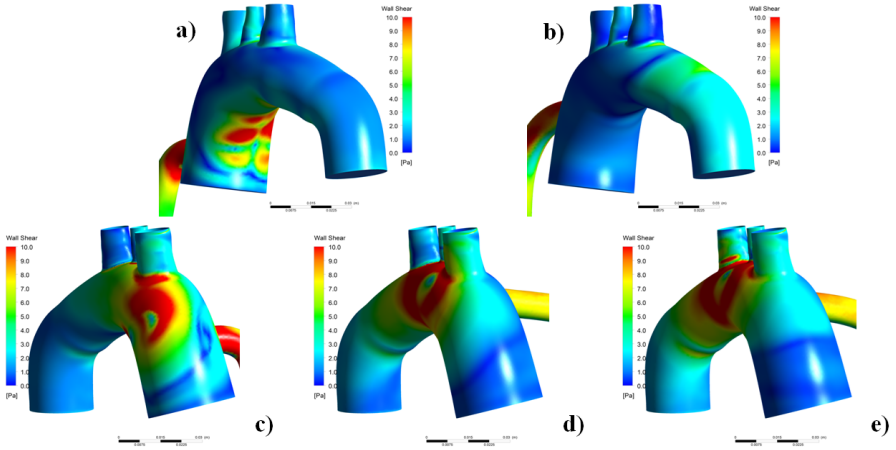

Figure 8 Wall shear stress distribution on the aortic arch - comparable analysis between different positioning of the LVAD outflow cannula

4. Discussion

One of the research purposes was to verify whether custom-created software, MeMoS, can enhance the anatomical models reconstruction processes and generate files compatible with CAD (i.e. SolidWorks) and CFD (i.e. Ansys CFX) software. Since the patient-specific arterial model was reconstructed and LVAD outflow cannula was easily attached to the obtained geometry, one can state that MeMoS is a viable

software for the vessel tree network data extraction.

The main objective of the following research was to analyze the impact of the LVAD outflow cannula positioning on the blood distribution among the brain-supplying arteries. Majority of publications that focus on the LVAD anastomosis outline data concerning the ascending aorta or descending aorta. Numerous authors investigate the wall shear stress distribution, pressure and velocity inside the aortic arch and descending aorta [7, 15-18]. However, only two publications focused on how the cannula positioning influences the blood distribution among the supra-aortic branches, i.e. brachiocephalic trunk, left common carotid and left subclavian arteries [4, 6]. The results of the first publication showed that the negative flow was present in the carotid artery, what might contribute to the negative flow in the cerebral circulation and, as a consequence, to the brain ischemia [4].

The numerical analyses performed within this research assumed insufficiently operating heart, however, generating weak pulses - the peak velocity of each pulse (occurring during systole) was equal to 0.1 m/s, what corresponds to approximately 10% of the physiological inflow. The remaining part of the physiological value of the cardiac output was sustained by the constant inflow from the LVAD outflow cannula, $7.5{\cdot}10^{-5}$ m^3/s (4.5 liter per minute). Similar approach was presented in the study of Karmonik et al. (2014), who assumed 5% of the total inflow through the aorta inlet. Prior to comparing the obtained results with the similar studies, the authors had to verify whether the computed data is in conformity with the physiological values for the analyzed vascular system. Having calculated the mean values of the volume flow rate together with their standard deviations for the internal carotid and vertebral arteries, the authors could compare those results with the statistical analysis found in the literature (please see Table 3).

Table 3 Obtained volume flow rates at several arteries compared with the literature, statistical data [28, 29]

Artery type	CFD results [cm^3/s]	Color Doppler USG [cm^3/s]	Power Doppler USG [cm^3/s]	B-flow USG [cm^3/s]	MR PC [cm^3/s]
Internal carotid	Right: 3.67 ± 0.08 Left: 3.86 ± 0.11	5.10 ± 2.20	5.28 ± 1.97	3.98 ± 1.55	3.60 ± 1.38
Vertebral	Right: 1.27 ± 0.01 Left: 1.86 ± 0.04	1.27 ± 0.62	1.42 ± 0.77	0.85 ± 0.47	0.75 ± 0.40 1.30-5.27
USG - Ultrasonography Examination MR PC - Magnetic Resonance Imaging with Phase Contrast					

As can be observed, all the data are in conformity with the physiological ranges found in the literature. Thus, it indicates that the numerical simulations conducted within this research resemble the natural, physiological flow and can be compared with further studies.

The experimental study of Laumen et al. (2010) shows that the outflow cannula positioning directly influences the blood flow in the greater vessels - even the negative flow was present in the right carotid artery, what might lead to the reduction in the cerebral perfusion [4]. The influence of the anastomosis location on the blood flow was also confirmed by Caruso et al. (2015) [6]. Both groups of scientists claim that one could observe the changes in the blood flow patterns in the ascending aorta and in the supra-aortic vessels, due to different anastomosis locations. Contrary to the aforementioned, the study of Bonnemain et al. (2013), who examined different locations of the cannula anastomosis (in ascending and descending aorta) and different rotational speeds of the pump, shows that despite varied cannulation locations, obtained waveforms were similar [2].

Concerning the own numerical results (presented in Table 2 and Table 3), it can be undoubtedly stated that the volume flow rate inside each brain-supplying artery (vertebral and internal carotid arteries, both left and right) is almost identical, notwithstanding the varied cannula anastomosis location. Therefore, it indicates that the LVAD outflow cannula positioning does not have a significant impact on the blood distribution among the brain-supplying arteries. The maximal discrepancy reached the value of 5% and was present in the case, where the jet stream from the cannula was directed towards the distal wall of the descending aorta. Own results of the volume flow rate were compared with the data obtained by the previously listed groups of scientists (please see Table 4).

Table 4 Obtained volume flow rates at several arteries compared with similar studies found in the literature

Artery type	CFD results [cm^3/s]	Laumen et al. results [4] [cm^3/s]	Caruso et al. results [6] [cm^3/s]	Bonnemain et al. results [2] [cm^3/s]
Common carotid	Right: 6.25 ± 0.18 Left: 6.11 ± 0.14	Right: -10.0 Left: 9.50	Left: 6.17	Right: 4.10 ± 0.39
Vertebral	Right: 1.27 ± 0.01 Left: 1.86 ± 0.04	Right: 1.17 Left: 4.83	-	Right: 0.89 ± 0.05
Left subclavian	6.03 ± 0.43	9.33	6.17	4.31 ± 0.40

As can be seen, the outlined values differ among each other, e.g. the only similarity of the own results with the Laumen et al. (2010) results is the flow in the right vertebral artery. The only similarity with the Caruso et al. (2015) results is the flow in left subclavian artery. There are several explanations of such discrepancies. The first one is connected with the imposed boundary conditions - not only Laumen et al. (2010) and Caruso et al. (2015) did not assume any inflow through the aorta inlet (contrary to this study, where 10% of total inflow passes through the aortic valves), but also they used different pressure values imposed on the outlets. The second aspect that could play a significant role when it comes to the presented differences, was the cannulation location - Laumen et al. (2010) assumed the anastomosis at right subclavian artery, whereas this study focused on

the cannulation at the ascending aorta. Nevertheless, both Laumen et al. (2010) and Caruso et al. (2015) did not specify the exact differences between investigated cases - they claim that the cannulation location influences the flow in ascending aorta and supra-aortic arteries, however, the numerical data of those differences are not outlined. Therefore, it cannot be stated whether the presented results differ by less than 3%, 5%, 10% or more than 10%. If the discrepancies are lower than 5%, those changes can be treated as negligible.

As far as the WSS in the aortic arch is concerned, it can be stated that the outflow cannula positioning influences its distribution on the vessel wall. Almost in every single analyzed case, apart from the VAD b (where the jet stream is directed into the lumen of the ascending aorta and to the descending aorta), the values of the WSS exceeded the presumably physiological range. Obtained values were even 10 times higher (over 10 Pa) than the upper limit of the physiological range, i.e. 1.0 Pa [9, 25]. Since the elevated WSS might result with severe complications for the patient's health, it's advisable to anastomose the cannula at the most optimal location and with the most optimal angle. It proves that the cannula positioning is a crucial aspect when the WSS distribution is concerned. Such a conclusion is in conformity with numerous publications found in the literature [6, 7, 9].

Due to some limitations of the current, standard diagnostic techniques (e.g. computed tomography or magnetic resonance imaging), calculation or prediction of the WSS is a problematic aspect, thus, the best way to estimate this parameter is to use the numerical simulations encompassing the patient-specific models. The numerical analyses conducted before the implantation of the LVAD might give an insight for the physicians about the most optimal implantation location.

5. Conclusions

It was proven that the custom-created software, modified version of MeMoS [19], supports the vascular tree network models reconstruction and exports data compatible with the CAD and CFD software.

Performed numerical analyses indicated that the location of the LVAD outflow cannula is of significant importance when it comes to the flow parameters in the aortic arch (mainly affecting velocity and wall shear stress distribution). Hence, by testing numerous cases with the different cannulas anastomosis and with varied inclination angles, physicians could estimate the most optimal LVAD outflow cannula configuration for the specific patient.

However, contrary to the aforementioned, hardly any changes in the flow distribution in the brain-supplying arteries (vertebral and internal carotid) could be observed. This means that the cannula anastomosis location does not contribute to significant changes in the blood distribution to the brain-supplying arteries - despite varied LVAD cannulas configurations, the volume flow rate in each of the indicated arteries was almost identical, with the maximal variation equal to approximately 5%. As opposed to the work of Laumen et al. (2010), the authors did not obtain the negative flow in one of the carotid arteries - conducted numerical analyses do not indicate that specific configuration of the LVAD outflow cannula might contribute to the reduction of the cerebral perfusion and occurrence of the brain ischemia.

References

[1] **Benjamin, E. J., Blaha, M. J., Chiuve, S. E., Cushman, M., Das, S. R., Deo, R., and Jiménez, M. C.**: Heart disease and stroke statistics-2017 update: a report from the American Heart Association, *Circulation*, 135, 10, e146-e603, **2017**.

[2] **Bonnemain, J., Malossi, A. C. I., Lesinigo, M., Deparis, S., Quarteroni, A., and von Segesser, L. K.**: Numerical simulation of left ventricular assist device implantations: comparing the ascending and the descending aorta cannulations, *Med. Eng. Phys.*, 35, 10, 1465-1475, **2013**.

[3] **Thunberg, C.A., Gaitan, B.D., Arabia, F.A., Cole, D.J., and Grigore, A.M.**: Ventricular assist devices today and tomorrow, *J Cardiothor Vasc An*, 24, 4, 656–680, **2010**.

[4] **Laumen, M., Kaufmann, T., Timms, D., Schlanstein, P., Jansen, S., Gregory, S., ... and Steinseifer, U.**: Flow analysis of ventricular assist device inflow and outflow cannula positioning using a naturally shaped ventricle and aortic branch, *Artif Organs*, 34, 10, 798–806, **2010**.

[5] **Fraser, K. H., Taskin, M. E., Griffith, B. P., and Wu, Z. J.**: The use of computational fluid dynamics in the development of ventricular assist devices, *Med Eng Phys*, 33, 3, 263–280, **2011**.

[6] **Caruso, M. V., Gramigna, V., Rossi, M., Serraino, G. F., Renzulli, A., and Fragomeni, G.**: A computational fluid dynamics comparison between different outflow graft anastomosis locations of Left Ventricular Assist Device (LVAD) in a patient-specific aortic model, *Int. J. Numer. Meth. Bio.*, 31, 2, **2015**.

[7] **Karmonik, C., Partovi, S., Loebe, M., Schmack, B., Weymann, A., Lumsden, A. B. and Ruhparwar, A.**: Computational fluid dynamics in patients with continuous-flow left ventricular assist device support show hemodynamic alterations in the ascending aorta, *J Thorac Cardiov Sur*, 147, 4, 1326–1333, **2014**.

[8] **Patil, N. P., Sabashnikov, A., Mohite, P. N., Garcia, D., Weymann, A., Zych, B. and De Robertis, F.**: De novo aortic regurgitation after continuous-flow left ventricular assist device implantation, *Ann Thorac Surg*, 98, 3, 850–857, **2014**.

[9] **Callington, A., Long, Q., Mohite, P., Simon, A., and Mittal, T. K.**: Computational fluid dynamic study of hemodynamic effects on aortic root blood flow of systematically varied left ventricular assist device graft anastomosis design, *J Thorac Cardiov Sur*, 150, 3, 696–704, **2015**.

[10] **Schmid, C., Jurmann, M., Birnbaum, D., Colombo, T., Falk, V., Feltrin, G. and Gummert, J.**: Influence of inflow cannula length in axial-flow pumps on neurologic adverse event rate: results from a multi-center analysis, *J Heart Lung Transpl*, 27, 3, 253–260, **2008**.

[11] **DiGiorgi, P. L., Smith, D. L., Naka, Y., and Oz, M. C.**: In vitro characterization of aortic retrograde and antegrade flow from pulsatile and non-pulsatile ventricular assist devices, *J Heart Lung Transpl*, 23, 2, 186–192, **2004**.

[12] **Nawata, K., Nishimura, T., Kyo, S., Hisagi, M., Kinoshita, O., Saito, A. and Ono, M.**: Outcomes of midterm circulatory support by left ventricular assist device implantation with descending aortic anastomosis, *J Artif Organs*, 13, 4, 197–201, **2010**.

[13] **Verdonck, P. R., Siller, U., De Wachter, D. S., De Somer, F., and Van Nooten, G.**: Hydrodynamical comparison of aortic arch cannulae, *Int J Artif Organs*, 21, 11, 705–713, **1998**.

[14] **Kapetanakis, E. I., Stamou, S. C., Dullum, M. K., Hill, P. C., Haile, E., Boyce, S. W. and Corso, P. J.**: The impact of aortic manipulation on neurologic

outcomes after coronary artery bypass surgery: a risk-adjusted study, *Ann Thorac Surg*, 78, 5, 1564–1571, **2004**.

[15] **Kaufmann, T. A. S., Schmitz-Rode, T., Moritz, A., and Steinseifer, U.**: Effect of outflow cannula placement and pulsatility of blood pumps on cerebral blood flow and wall shear stress during cardiac assist, *Blucher Mech Eng Proc*, 822–835, **2012**.

[16] **May-Newman, K., Hillen, B., and Dembitsky, W.**: Effect of left ventricular assist device outflow conduit anastomosis location on flow patterns in the native aorta, *ASAIO journal*, 52, 2, 132–139, **2006**.

[17] **Yang, N., Deutsch, S., Paterson, E.G., and Manning, K.B.**: Numerical study of blood flow at the end-to-side anastomosis of a left ventricular assist device for adult patients, *J Biomech Eng*, 131, 11, 111005, **2009**.

[18] **Kar, B., Delgado III, R. M., Frazier, O. H., Gregoric, I. D., Harting, M. T., Wadia, Y. and Freund, J.**: The effect of LVAD aortic outflow-graft placement on hemodynamics and flow: implantation technique and computer flow modeling, *Tex. Heart. I. J.*, 32, 3, 294, **2005**.

[19] **Tyfa, Z. and Strzelecki, M.**: MeMoS—A software tool for extraction of anatomical structures data from 3D medical images, In *Signal Processing: Algorithms, Architectures, Arrangements, and Applications (SPA)*, 97–102, IEEE, **2016**.

[20] **Jóźwik, K., and Obidowski, D.**: Numerical simulations of the blood flow through vertebral arteries, *J. Biomech.*, 43, 177–185, **2010**.

[21] **Reorowicz, P., Obidowski, D., Klosiński, P., Szubert, W., Stefańczyk, L. and Jóźwik, K.**: Numerical simulations of the blood flow in the patient-specific arterial cerebral circle region, *J Biomech*, 47, 1642–1651, **2014**.

[22] **Tyfa, Z., Obidowski, D., Reorowicz, P., Stefańczyk, L., Fortuniak, J., and Jóźwik, K.**: Numerical simulations of the pulsatile blood flow in the different types of arterial fenestrations: Comparable analysis of multiple vascular geometries, *Biocybern Biomed Eng*, 38, 2, 228–242, **2018**.

[23] **Bochenek, A., and Reicher, M.**: Human Anatomy, III, *PZWL, Warsaw*, (in Polish), **1974**.

[24] **Michajlik, A., Ramotowski, W.**: Human Anatomy and Physiology, *PZWL, Warsaw*, (in Polish), 354–356, **1996**.

[25] **Meierhofer, C., Schneider, E. P., Lyko, C., Hutter, A., Martinoff, S., Markl, M. and Fratz, S.**: Wall shear stress and flow patterns in the ascending aorta in patients with bicuspid aortic valves differ significantly from tricuspid aortic valves: a prospective study, *Eur Heart J Cardiovasc Imaging*, 14, 8, 797–804, **2012**.

[26] **Uchino, A., Sawada, A., Takase, Y., Fujita, I.and Kudo, S.**: Extreme fenestration of the basilar artery associated with cleft palate, nasopharyngeal mature teratoma, and hypophyseal duplication, *Eur Radiol*, 12, 8, 2087–2090, **2002**.

[27] **Rennert, J., Ullrich, W. O. and Schuierer, G.**: A rare case of supraclinoid internal carotid artery (ICA) fenestration in combination with duplication of the middle cerebral artery (MCA) originating from the ICA fenestration and an associated aneurysm, *Clin Neuroradiol*, 23, 2, 133-136, **2013**.

[28] **Oktar, S. O., Yücel, C., Karaosmanoglu, D., Akkan, K., Ozdemir, H., Tokgoz, N. and Tali, T.**: Blood-flow volume quantification in internal carotid and vertebral arteries: comparison of 3 different ultrasound techniques with phase-contrast MR imaging, *Am J Neuroradiol*, 27, 2, 363–369, **2006**.

[29] **Ford, M. D., Alperin, N., Lee, S. H., Holdsworth, D. W. and Steinman, D. A.**: Characterization of volumetric flow rate waveforms in the normal internal carotid and vertebral arteries, *Physiol meas*, 26, 4, 477, **2005**.